Enhanced optical tuning of modified-geometry resonators clad in blue phase liquid crystals

Joanna Ptasinski,[1,2,*] Iam-Choon Khoo,[3] and Yeshaiahu Fainman[1]

[1]*Department of Electrical and Computer Engineering, University of California San Diego, La Jolla, California 92037, USA*

[2]*Space and Naval Warfare Systems Center Pacific, San Diego, California 92152, USA*

[3]*Electrical Engineering Department, Pennsylvania State University, University Park, Pennsylvania 16802, USA*

**Corresponding author: jptasins@ucsd.edu*

Received July 4, 2014; accepted August 8, 2014;
posted August 19, 2014 (Doc. ID 216364); published September 15, 2014

Active optical tuning of silicon racetrack resonators clad in dye-doped blue phase liquid crystals (BPLCs) is experimentally demonstrated. An adiabatic racetrack resonator geometry that allows for enhanced tuning is presented and analyzed. The resonance shift of an unmodified geometry racetrack is $\Delta\lambda = 0.7$ nm, while an adiabatic racetrack achieves a $\Delta\lambda = 1.23$ nm resonance shift because of a greater mode overlap with the cladding. The calculated refractive index change of the BPLC is $\Delta n = 0.0041$ for both geometries. © 2014 Optical Society of America

OCIS codes: (130.2790) Guided waves; (130.3120) Integrated optics devices; (130.3130) Integrated optics materials; (160.3710) Liquid crystals; (160.5320) Photorefractive materials; (220.0220) Optical design and fabrication.
http://dx.doi.org/10.1364/OL.39.005435

Tunable optical circuit components are one of the essential technologies in the development of photonic analogues for classical electronic devices, since using one tunable device replaces many single wavelength devices and therefore minimizes the space occupied on-chip [1,2]. Tunable photonic resonant structures allow for altering of their electromagnetic spectrum and are found to be useful for realization of chip-scale devices for optical switching and modulation, filtering, buffering, and light emission leading to on-chip networking and biosensing applications. Examples of dielectric resonators include rings, racetracks, disks, waveguide grating resonators and contra-directional grating coupler ring resonators [3–5].

Blue phase liquid crystals (BPLCs) have garnered a considerable amount of attention because of their optical isotropy stemming from their three-dimensional self-assembled photonic band gap structure, and their electro-optical and nonlinear optical properties [6–12]. Unlike their nematic counterpart, BPLCs and their polymerized variants do not require surface alignment during fabrication, and can thus be easily integrated into various nonplanar structures such as capillary arrays [11], and photonic crystal fibers [12]. The blue phase electro-optic switching time is more than an order of magnitude faster than that of conventional nematics and they're being explored for next generation displays [7], sub-millisecond range polarization independent variable optical attenuators [8], and random lasers [9]; their recently discovered nonlinear optical properties have been utilized in all-optical wave-mixing and switching operations with cw-nanoseconds pulsed lasers [10,11].

Here, to the best of our knowledge, we are the first to show optical tuning of racetrack resonator structures using BPLC claddings. The liquid crystal (LC) was doped with methyl red dye and tuned by an unpolarized light source which induced a refractive index change on the waveguide surfaces [13], as we will explain in more detail in later discussions on the experimental results. Optical tuning offers the advantage of noncontact, electrode-free and configuration flexibility, and thus such optically tunable silicon photonic devices are likely to play an increasingly central role in all-optical circuit components realized with silicon photonic material platforms. Previously, optical tuning of ring resonators clad in nematic LCs using linearly polarized light was shown [13], but the ring resonator geometry limit modifications made to the waveguide width to achieve a greater optical mode overlap with the cladding without accruing a significant amount of loss.

In this Letter, we investigate and compare the performance of racetrack resonators designed in two geometries: (1) a typical racetrack where the waveguide geometry retains a 500 nm Si strip width over the entire perimeter, and (2) a racetrack where the Si waveguide is adiabatically thinned between 500 and 300 nm to allow for greater mode overlap with the LC cladding. The first structure consists of a 500 nm wide, 250 nm tall silicon racetrack resonator of 182.2 μm perimeter. The racetrack is positioned on top of a 3 μm thick buried oxide (BOX) layer. The curved portion of the racetrack is of a 9.9 μm radius. The resonant wavelength of this structure can be determined by considering the effective index n_{eff} of the waveguide mode and the racetrack perimeter L

$$\lambda_{\text{res}} = \frac{n_{\text{eff}} L}{m}, \qquad m = 1, 2, 3\ldots, \tag{1}$$

where m indicates the order. This racetrack structure is shown in Fig. 1(A).

Fig. 1(B) shows our second racetrack resonator with modified geometry design, where a portion of the racetrack is adiabatically narrowed from 500 to 300 nm in the course of 28 μm. A 300 nm wide waveguide portion is present over the course of 4 μm, and it adiabatically increases back to 500 nm. The entire path around the racetrack is 182.2 μm. The resonant wavelength of this structure is determined by taking into account the changing effective index as the racetrack is narrowed/widened

$$m\lambda_{\text{res}} = n_{\text{eff}500\text{ nm}} \cdot 2\pi R + 2n_{\text{eff}300\text{ nm}} \cdot L_{\text{center}} + 4n_{\text{eff}500\text{ nm}\to 300\text{ nm}} \cdot L_{\text{adiab}}, \tag{2}$$

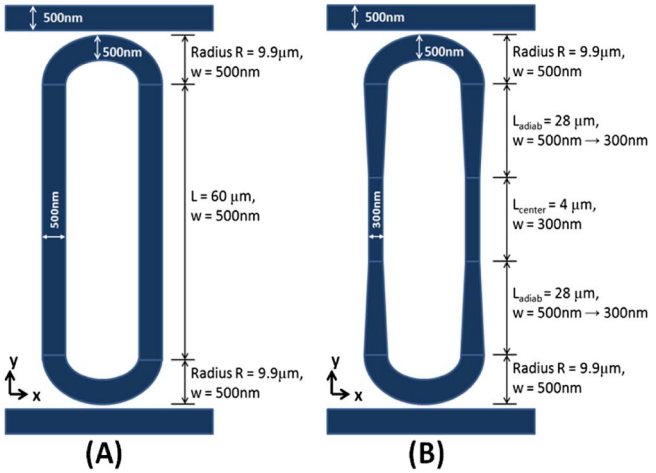

Fig. 1. (A) Nonadiabatic racetrack resonator. (B) Adiabatic racetrack resonator.

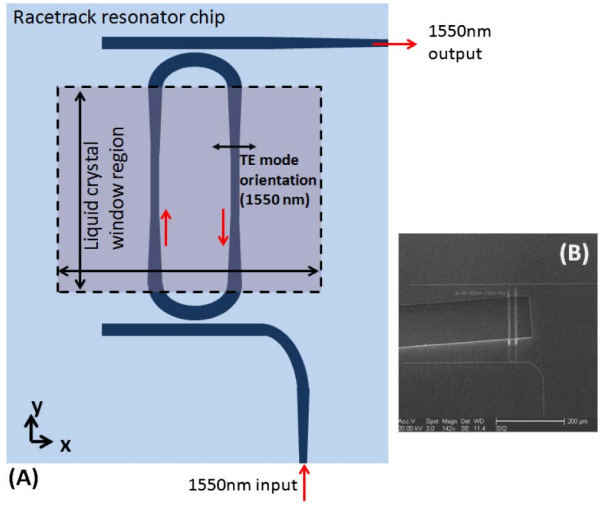

Fig. 2. (A) Conceptual schematic of the racetrack resonator showing where a window for LCs is etched into the SiO_2 cladding. The red arrows indicate the 1550 nm source propagation direction. (B) An SEM image of a fabricated resonator showing a window region for LCs.

where $n_{\text{eff\_500 nm}}$ refers to the effective index of a 500 nm wide waveguide, $n_{\text{eff\_300 nm}}$ is the effective index of a 300 nm waveguide, $n_{\text{eff\_500 nm}\to\text{300 nm}}$ is the effective index of the adiabatic portion, R is the ring radius, L_{center} is the length of the 300 nm-wide center portion, and L_{adiab} is the length of the adiabatic part. Similarly, the resonator quality factor can be described by

$$Q = \frac{[n_{\text{eff}500\text{ nm}} \cdot 2\pi R + 2n_{\text{eff}300\text{ nm}} \cdot L_{\text{center}}]}{\lambda} \cdot \frac{\text{FSR}}{\text{FWHM}} + \frac{[4n_{\text{eff}500\text{ nm}\to300\text{ nm}} \cdot L_{\text{adiab}}]}{\lambda} \cdot \frac{\text{FSR}}{\text{FWHM}}, \quad (3)$$

where FSR refers to the free spectral range and FWHM is the full width at half-maximum of the resonance.

A conceptual schematic of our sample appears in Fig. 2(A), where the 1550 nm source input and output are shown, as well as a window region for the LC cladding.

A scanning electron microscope (SEM) image of the structure is depicted in Fig. 2(B). Our racetrack resonators were fabricated using an SOI platform where Hydrogen silsesquioxane (HSQ) resist was patterned with electron beam lithography. After development, the HSQ served as a mask for the dry etch of silicon. The silicon structures were covered by a 1.8 um layer of SiO_2 cladding deposited via plasma-enhanced chemical vapor deposition (PECVD). Window areas for BPLCs were patterned using photolithography and etched in a buffered oxide solution [13]. The BPLC consisted of 32 wt. % of the nematic E48, 32 wt. % of the nematic 5CB and, 36 wt. % of the chiral dopant S811. This BPLC is similar to RT-35 [14], and the refractive index of this optically isotropic material system at 1550 nm and 25°C is $n = 1.52$. The BPLC was mixed with methyl red (MR) dye at ~0.1% concentration. A drop of LC material was placed onto the window regions of the sample and heated at 37°C (above the clearing temperature of the BPLC mixture), then cooled back to room temperature. This step aided in the LC material completely filling the cell, and was performed with the aid of a thermoelectric module embedded inside the sample mount and controlled via an Oven Industries 5C7-195 Benchtop Temperature Controller. A thermocouple fastened to the sample stage monitored the temperature to within 0.1°C precision. The optical setup consisted of a tunable 1470–1570 nm laser and a polarizer in the output path allowed for selection of TE transmission (horizontal polarization) or TM transmission (vertical polarization). The optical setup is shown in Fig. 3.

Measurements were performed with TE polarized light in the fundamental mode of the waveguide. Control of the telecom source, the power meter, and the source step size was automated. An unpolarized Mightex LED source was focused onto the sample with a plano-convex lens resulting in a spot size of 0.49 cm^2. The wavelength of the source was chosen to coincide with the MR dye absorption spectrum. The output power irradiating the sample was 0.5 mW. Figures 4–7 show our measured results. Figures 4,5 are the measured spectra of an unmodified racetrack resonator with BPLC and the adiabatically thinned racetrack clad in BPLC, respectively. The FSR of an unmodified racetrack is 3.1 nm, and the modified

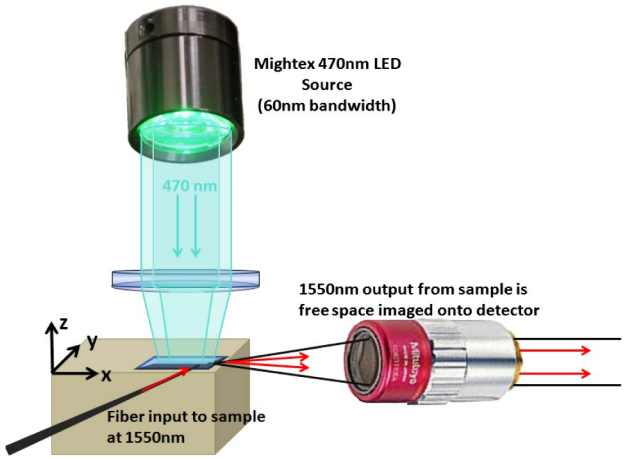

Fig. 3. Optical setup showing sample placement with respect to the 470 nm source and the 1550 nm source. The 1550 nm light is fiber coupled to the sample, and free space is imaged at the output.

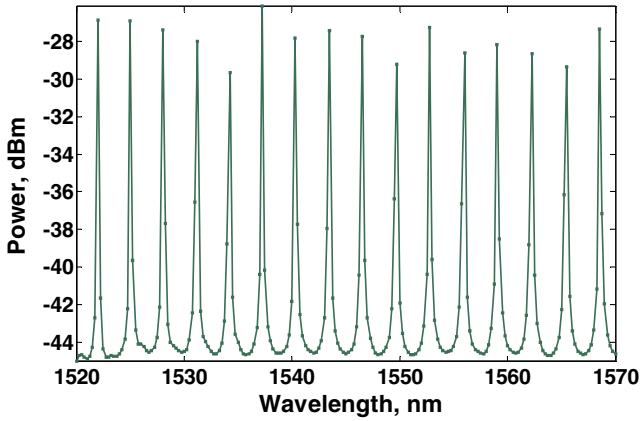

Fig. 4. Measured spectral response of a nonadiabatic racetrack. The FSR = 3.1 nm.

racetrack results in a FSR of 3.15 nm. The phototuning response of the dye-doped BPLC is shown in Figs. 6 and 7. The measurements were taken over time and stopped upon saturation. The total 470 nm source dosage was calculated and the resonance shift was plotted as a function of energy density. For 500 nm wide waveguides, the total resonance shift was 0.7 nm and the response saturated beginning at 40 J/cm^2. Waveguides with modified geometry yielded a considerably larger resonance shift of 1.23 nm, and saturation occurred at 30 J/cm^2. The unmodified racetrack Q is 6,150; while the modified racetrack geometry results in a slightly lower Q of 5,200. The sharpness of the resonator Q depends on loss, and we attribute the modified racetrack resonator losses to fabrication errors associated with achieving a perfectly adiabatic waveguide region (i.e., sidewall roughness) and a higher amplitude value of the mode being present on the rough boundary.

To calculate the refractive index change of the LC as a result of phototuning, simulations were performed using COMSOL Multiphysics. The measured resonance shifts served to compute the effective index change for each racetrack geometry, and the effective indices were then used to come up with the LC refractive index change for each geometric configuration. These results are shown in Figs. 8, 9. Figure 8 depicts the resonance shift for an unmodified resonator geometry. The resonance peak

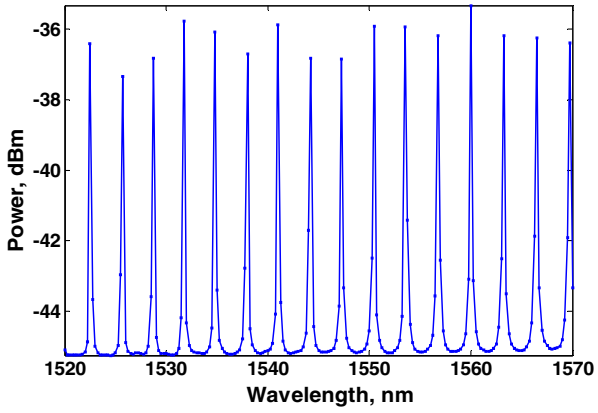

Fig. 5. Measured spectral response of an adiabatic racetrack. The FSR = 3.15 nm

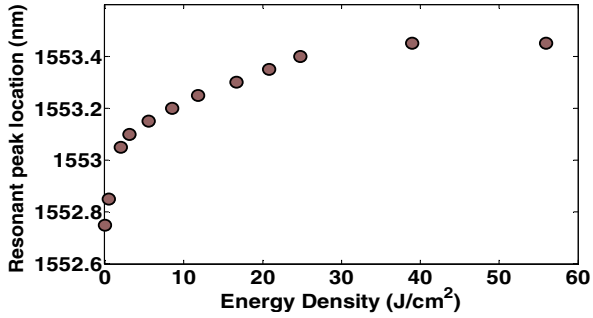

Fig. 6. Optical tuning of the nonadiabatic racetrack. The total resonance shift is 0.7 nm.

at the beginning of the experiment is represented by the blue curve and it occurs at $\lambda = 1549.5$ nm. The maximum possible resonance shift $\Delta\lambda_{max} = 1.7$ nm because of tuning of the BPLC, and corresponding to $\Delta n = 0.01$, is the difference between the red and the blue curve. The green curve, centered at $\lambda = 1550.2$ nm, represents the total resonance shift observed during our experiment. Similarly, Fig. 9 shows the resonance shifts associated with the modified geometry racetrack. The blue curve at $\lambda = 1556.77$ nm represents the resonance peak at the beginning of the experiment. The maximum expected resonance shift is $\Delta\lambda_{max} = 3.0$ nm, and the observed resonance shift $\Delta\lambda_{obs} = 1.23$ nm is the difference between the magenta and the blue curve. It can be deduced from both measurements that the refractive index change of the optically tuned BPLC was $\Delta n = 0.0041$.

The modified geometry racetrack showed a considerable, 76%, improvement in the tuning range for a $\Delta n =$

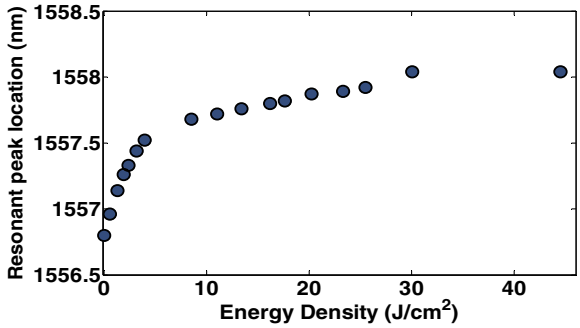

Fig. 7. Optical tuning of the adiabatic racetrack. The total resonance shift is 1.23 nm.

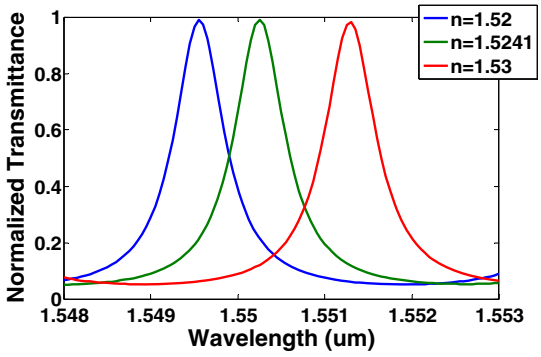

Fig. 8. Simulation results for the tuning range of the nonadiabatic racetrack resonator.

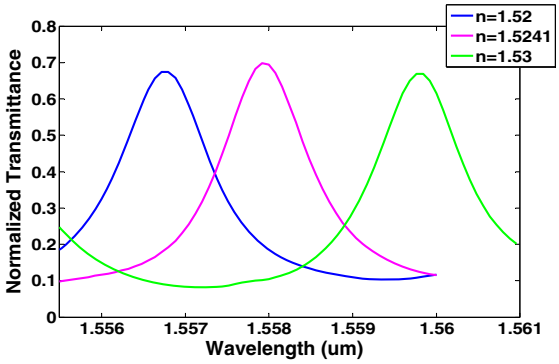

Fig. 9. Simulation results for the tuning range of the adiabatic racetrack resonator.

0.0041 change in the refractive index of the cladding. The adiabatic geometry allows for an increased optical mode interaction with the cladding material while minimizing losses associated with mode confinement around bends, minimum allowed bend radius, and coupling between adjacent waveguides [3]. Saturation in the case of the modified racetrack resonators occurred slightly sooner as compared to the unmodified racetracks (Figs. 6,7).

We attribute the refractive index change to the surface anchoring modification effects by the laser excited MR dye-molecules. As observed in other studies, [15–18], when photo-excited, methyl-red doped liquid crystalline materials exhibit two principal phenomena, one occurring in the bulk, and one on the surface [15]: (a) Light absorption and photoisomerization in the bulk producing Cis-state molecules gives rise to optical torque on the LCs director pushing the easy axis away from the light polarization direction; this gives negative nonlinearity observed in the grating diffraction experiments involving bulk BPLC [10]; (b) Excited Cis-state dye-molecules are adsorbed on the waveguide surface pushing the easy axis toward the light polarization direction. In the present case, the electric fields on the LC/waveguide interfaces consists of the randomly polarized pump laser and the evanescent field from the TE polarized waveguides modes, and therefore the easy axis is predominantly along the x-direction; the induced index change as sensed by the polarized TE waveguides modes is therefore positive in sign [15,16], as observed in this experiment. Similar to other surface adsorption mediated effects observed in MR-doped liquid crystalline systems [10,18], this adsorption induced director axis alignment on the surface can assume a persistent nature once it is built up. This was also borne out in our study; upon prolonged illumination, the resonance shift exhibited a component that persisted for tens of minutes when the excitation source was turned off.

In summary, we have shown optical tuning of silicon photonic resonator structures clad in dye doped blue phase liquid crystals. The optical tuning was performed with unpolarized light and for two different resonator geometries. An adiabatic geometry Si strip racetrack resonator achieved a 76% greater tuning range versus an unmodified structure. The adiabatic geometry played a significant role in the tuning range of the resonator for a liquid crystal refractive index change of $\Delta n = 0.0041$ while aiding in the minimization of losses.

This work was supported by the Defense Advanced Research Projects Agency, the Air Force Office of Scientific Research, the National Science Foundation Center for Integrated Access Networks, the Office of Naval Research Multidisciplinary University Initiative, and by SPAWAR Systems Center Pacific. We thank Professor Tsung-Hsien Lin for providing the blue phase liquid crystal indices at 1550 nm and for helpful discussions. We thank the Nano3 staff for ebeam exposure.

References

1. J. Cos, J. Ferré-Borrull, J. Pallarès, and L. F. Marsal, Phys. Status Solidi C **8**, 1075 (2011).
2. V. R. Almeida, C. A. Barrios, R. R. Panepucci, and M. Lipson, Nature **431**, 1081 (2004).
3. S. Janz, J. Ctyroky, and S. Tanev, *Frontiers in Planar Lightwave Circuit Technology: Design, Simulation, and Fabrication* (Springer Verlag, 2006), Chap. 1.
4. S. Zamek, D. Tan, M. Khajavikhan, M. Ayache, M. Nezhad, and Y. Fainman, Opt. Lett. **35**, 3477 (2010).
5. S. Grist, S. Schmidt, J. Flueckiger, V. Donzella, W. Shi, S. Talebi Fard, J. Kirk, D. Ratner, K. Cheung, and L. Chrostowski, Opt. Express **21**, 7994 (2013).
6. A. Yoshizawa, RSC Adv. **3**, 25475 (2013).
7. H. Kikuchi, M. Yokota, Y. Hiskado, H. Yang, and T. Kajiyama, Nat. Mater. **1**, 64 (2002).
8. G. Zhu, B. Wei, L. Shi, X. Lin, W. Hu, Z. Huang, and Y. Lu, Opt. Express **21**, 5332 (2013).
9. C. W. Chen, H. C. Jau, C. T. Wang, C. H. Lee, I. C. Khoo, and T. H. Lin, Opt. Express **20**, 23978 (2012).
10. I. C. Khoo and T. H. Lin, Opt. Lett. **37**, 3225 (2012).
11. I. C. Khoo, K. L. Hong, S. Zhao, D. Ma, and T. H. Lin, Opt. Express **21**, 4319 (2013).
12. C. H. Lee, C. W. Wu, C. W. Chen, H. C. Jau, and T. H. Lin, Appl. Opt. **52**, 4849 (2013).
13. J. Ptasinski, S. W. Kim, L. Pang, I. C. Khoo, and Y. Fainman, Opt. Lett. **38**, 2008 (2013).
14. C. W. Chen, H. C. Jau, C. H. Lee, C. C. Li, C. T. Hou, C. W. Wu, T. S. Lin, and I. C. Khoo, Opt. Mater. Express **3**, 527 (2013).
15. L. Lucchetti and F. Simoni, Phys. Rev. E **89**, 032507 (2014).
16. E. Ouskova, Yu. Reznikov, S. V. Shiyanovskii, L. Su, J. L. West, O. V. Kuksenok, O. Francescangeli, and F. Simoni, Phys. Rev. E **64**, 051709 (2001).
17. I. C. Khoo, S. Slussarenko, B. D. Guenther, M. Y. Shih, P. Chen, and W. V. Wood, Opt. Lett. **23**, 253 (1998).
18. I. C. Khoo, M. Y. Shih, M. V. Wood, B. D. Guenther, P. H. Chen, F. Simoni, S. Slussarenko, O. Francescangeli, and L. Lucchetti, Proc. IEEE **87**, 1897 (1999).